Preprint 33rd EU PVSEC

INFLUENCE OF DIFFERENT TRANSITION METAL CONTAMINATIONS ON DEGRADATION AND REGENERATION IN MC SI

Andreas Schmid, Annika Zuschlag, Daniel Skorka, Jakob Fritz, Clemens Winter, Giso Hahn
University of Konstanz, Department of Physics, 78457 Konstanz, Germany

ABSTRACT: Light and elevated temperature induced degradation (LeTID) affects significantly the performance of multicrystalline Silicon (mc-Si) solar cells. The underlying mechanisms of LeTID and following regeneration are still unknown and might depend on contaminations. To investigate the influence of different transition metals on the degradation and regeneration behavior, mc-Si ingots were intentionally contaminated in the Si melt with either 20 ppma Fe, Cu, Cr or a combination of Fe and Cu. Minority charge carrier lifetime (τ_{eff}) samples were processed and the degradation and regeneration behavior under illumination (0.9 ± 0.1 sun) and elevated temperature (75°C) is measured repetitively by time-resolved photoluminescence imaging (TR-PLI) at room temperature. The resulting minority charge carrier lifetime maps are analyzed and the effective defect concentration within one sample and also for differently contaminated samples were calculated. This approach leads to different defect generation rates for the differently contaminated samples, which might hint to an influence of different transition metals on the LeTID causing defect.
Keywords: Degradation, Multicrystalline Silicon, Impurities, Lifetime

1 INTRODUCTION

Multicrystalline (mc) Si PERC (passivated emitter and rear cell) solar cells, but also lifetime samples, show a strong degradation of minority charge carrier lifetimes under illumination at elevated temperatures (*e.g.* [1-4]), so-called light and elevated temperature induced degradation (LeTID). The observed degradation kinetics cannot be explained by the already known degradation mechanisms like BO-correlated defects or the dissociation of FeB pairs [1-3]. Also a regeneration process after degradation has been observed for solar cells [3] and lifetime samples [5]. The kinetics of degradation and regeneration is influenced by measurement conditions, like illumination and temperature (*e.g.* [3, 6]), while the underlying mechanisms causing the degradation and regeneration of mc-Si are still unknown. In literature, several authors speculate on possible degradation and regeneration mechanisms [4, 7-9]. For all of them, defects correlated with getterable impurities play a crucial role. While in [7] a movement of impurities towards the wafer surface is assumed as the mechanism of regeneration, in [4] it is pointed out that the degradation strength can be influenced by preceding effective gettering processes. Lifetime spectroscopy data also gave first hints on possible candidates responsible for the degradation due to the measured ratio of capture cross sections of the underlying lifetime limiting defects [8, 9]. In this study we investigate the influence of several transition metal impurities common in mc-Si materials by using mc-Si materials intentionally contaminated with different elements in the melt before crystallization.

2 EXPERIMENTAL

To investigate the influence of different transition metals on the degradation and regeneration process, four intentionally contaminated mc-Si ingots are compared. For the contaminated mc-Si materials, 20 ppma of Fe, Cu, Cr or a combination of Fe and Cu were intentionally introduced into the Si melt. The detrimental effect of transition metals on the minority charge carrier lifetime in Si materials is known and, *e.g.*, described in [10]. NAA (neutron activation analysis) results regarding the transition metal concentration of the here investigated materials are shown in [11]. In the middle of the ingots the concentration of the intentionally implemented impurities is in the range of $7\text{x}10^{14}$ cm^{-3} for the Cu content of the Cu contaminated ingot, $5\text{x}10^{13}$ cm^{-3} for the Fe concentration of the Fe contaminated ingot and $9\text{x}10^{12}$ cm^{-3} for the Cr concentration of the Cr contaminated ingot. Regarding the ingot intentionally contaminated with a combination of Fe and Cu, the resulting impurity contents are in the same range as for the material contaminated with only one of these species. Additionally, standard mc-Si material is processed and characterized for reference. To investigate samples with different contamination levels of the same transition metal impurity, mc-Si wafers from three different ingot heights are available, as impurities are unevenly distributed over the ingot height due to segregation.

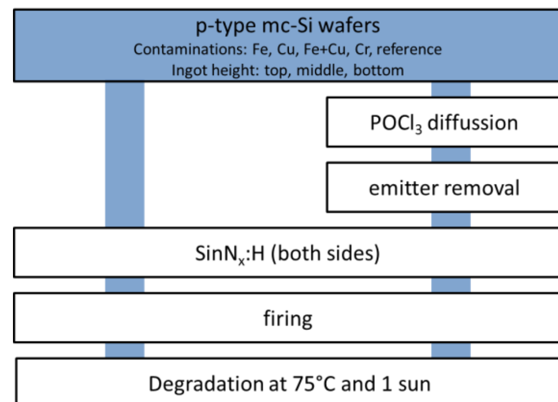

Figure 1: Process sequence of the investigated lifetime samples.

Sister wafers (only mid ingot height) of each contamination type with comparable grain and defect structure were used to compare the influence of the gettering step on the degradation and regeneration behavior of the lifetime sample. A scheme of the applied process sequences is given in Fig. 1. All samples were etched to remove the saw damage. On half of the wafers only a surface passivation was realized by firing of a PECVD (plasma-enhanced chemical vapor deposition) SiN_x:H layer. The sister wafers of these samples were gettered by a $POCl_3$ diffusion (55 Ω/□). Afterwards, the emitter was removed and the samples were also surface passivated by firing of a PECVD SiN_x:H layer.

For degradation, the samples are held at a temperature of approx. 75°C under illumination with halogen lamps (0.9 ± 0.1 sun). Minority charge carrier lifetime τ_{eff} is measured repetitively by the fast and self-calibrated TR-PLI method [12] at room temperature, resulting in a series of spatially resolved lifetime maps for each sample over degradation time. For a statistically relevant analysis of areas differing in material quality, an array of 2,500 areas (each 150x150 μm^2 in size) is distributed over the TR-PLI lifetime map of the 5x5 cm^2 mc-Si samples. Average τ_{eff} values within these areas are extracted over degradation time and further analyzed. This method allows tracking of changes in τ_{eff} of different sample areas under degradation conditions. The advantage of this approach is that the complete information of the spatially resolved τ_{eff} maps over degradation time can be easily displayed. The τ_{eff} data for each 150x150 μm^2 area on the samples is plotted over time and coded by a rainbow color bar based on the areas' lifetime values at the beginning of the degradation experiment (*cf.* [4]).

3 RESULTS

The harmonic average τ_{eff} for four different contaminated lifetime samples from middle ingot regions are shown in Fig. 2. All shown samples have been P-gettered. The ungettered samples showed initial lifetimes between 1 and 10 µs only and nearly no LeTID effect can be observed on such low lifetime levels. The P-gettering process reduces the contamination level, so that the overall minority charge carrier lifetime is significantly higher and LeTID as well as regeneration processes are easier to investigate.

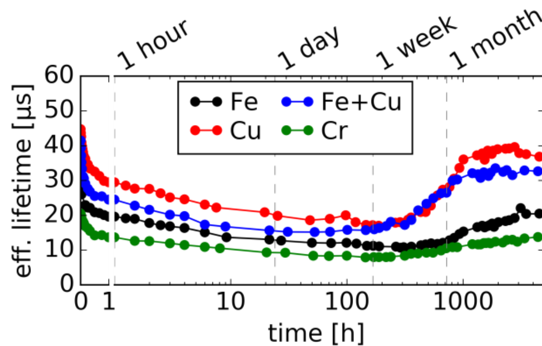

Figure 2: Harmonic average τ_{eff} data for differently contaminated mc-Si wafers. Degradation and regeneration behavior of lifetime samples can be strongly influenced by contamination type.

As expected, initial harmonic average τ_{eff} is lowest for Cr, slightly higher for Fe (both around 25 µs), and highest for Cu contaminated samples. As Cu is forming co-precipitates with Fe, the initial τ_{eff} of the Fe+Cu sample is closer to the only Cu contaminated sample (both around 45 µs) than to the only Fe contaminated one. These differences in the initial harmonic average τ_{eff} can be explained by different effects depending on the contamination type and the resulting gettering efficacy. The transition metals segregate differently during the cooling down of the Si in the ingot (internal gettering and formation of precipitates according to temperature dependent diffusivity and solubility). Furthermore, the higher the diffusion coefficient of the transition metal, the better the intentional contamination is reduced during the applied P-gettering step. Here the local grain structure of the sample becomes important for the distribution of contaminations (internal gettering).

Fig. 2 shows clearly that LeTID and regeneration is observed in all samples. Comparing the degradation behavior, the slight differences between the materials contaminated with Cu and a combination of Fe and Cu hint already on different degradation kinetics in dependence of the impurity species. Beside the degradation kinetics, also the strength of degradation is influenced by the different transition metal contents. For the regeneration effect different onsets and regeneration strengths were observed and seem to depend on contamination, too.

The disadvantage of average τ_{eff} analyses is that information on local τ_{eff} distribution measured by spatially resolved TR-PLI gets lost. Therefore, further analyses of the degradation and regeneration behavior will be exemplarily discussed in more detail based on the Fe+Cu contaminated sample shown in Fig. 3. The following description of the observed degradation and regeneration behavior holds true also for samples originating from mid ingot heights of the other intentionally contaminated samples.

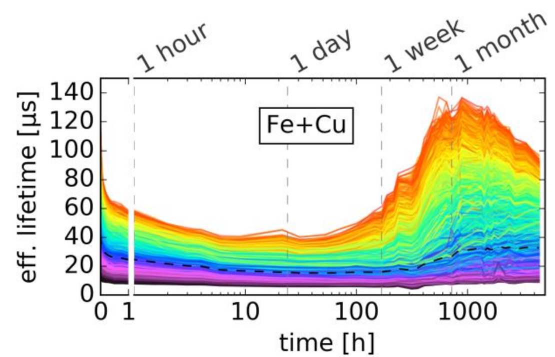

Figure 3: τ_{eff} for the Fe+Cu contaminated mc-Si wafer (x-axis: 0-1 h linear scale, 1-5,000 h log scale). Each line in the graph represents an area of 150x150 μm^2 in the spatially resolved TR-PLI lifetime measurements and is color-coded to its value at the beginning of degradation.

Each single line in Fig. 3 represents one of the 2,500 small areas on the lifetime samples as described above. The applied color code, based on the initial τ_{eff} of each sample at the beginning of the experiment, shows that the

relative τ_{eff} distribution is almost kept constant within each sample during the experiment, which means that sample areas with the highest initial τ_{eff} show also the highest τ_{eff} at the maximum degradation level as well as during the regeneration process. This holds true even if the range of lifetime is narrowed down during degradation or is spread again during regeneration as already described by [4] for standard industrial mc-Si.

After approximately 50 h a regeneration process sets in, with regeneration in areas with higher initial τ_{eff} (red lines) starting significantly earlier than in areas of lower initial τ_{eff} at maximum degradation level, again in good agreement with industrial mc-Si as described in [4]. In contrast to [4], τ_{eff} of some areas, mainly areas with high initial τ_{eff}, exceeds the initial τ_{eff}. It has to be mentioned that the sample shown in Fig. 2 has a lower τ_{eff} level due to the remaining impurity content compared to samples shown in [4]. After approximately 1,000 h a second decrease in τ_{eff} sets in. As stated in [4, 13] this behavior can be attributed to a decreasing surface passivation quality which limits the τ_{eff} values.

To investigate the influence of the local defect structure on the LeTID and regeneration behavior, all sample areas with 50 and 100 µs initial τ_{eff} are extracted from the rainbow plot shown in Fig. 3. The chosen sample areas (more than 200 pixels in the TR-PLI map for each of the chosen initial τ_{eff} values) are distributed all over the lifetime sample representing areas with same initial τ_{eff} but different defect structure. As the degradation behavior of areas with the same initial τ_{eff} is very similar, an influence of the local defect structure can be excluded. Additionally, the comparable behavior of different sample areas with the same initial τ_{eff} hints on the same root-cause of degradation even if the local defect structure is different.

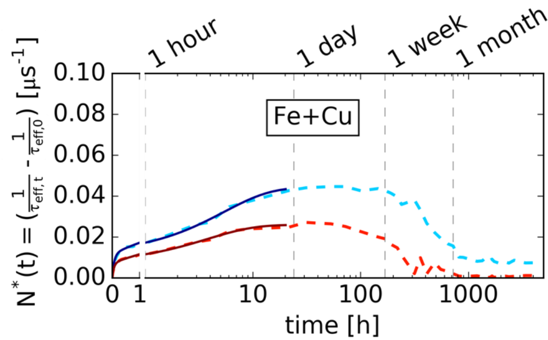

Figure 4: Time-dependent effective defect concentration of the Fe+Cu contaminated sample. The dotted red line represents all areas with 100 µs initial τ_{eff}, the dotted blue line all areas with 50 µs initial τ_{eff}. The solid lines show the exponential fit curves of the degradation.

To further quantify these observations, the harmonic average τ_{eff} of the extracted curves with initial τ_{eff} of 50 and 100 µs were calculated. Out of these data, the time-dependent effective defect concentration $N^*(t)$ is determined by

$$N^*(t) = \left(\frac{1}{\tau_{eff,t}} - \frac{1}{\tau_{eff,0}} \right)$$

and is shown in Fig 4. For degradation, it is possible to fit $N^*(t)$ within one sample with two saturating exponential functions with the same parameters. This is exemplarily shown at the Fe+Cu contaminated sample in Fig. 4, where the solid lines represent the fit-curves of the different initial τ_{eff}. Despite probably slightly different injection levels for areas with different initial τ_{eff}, this leads to comparable defect generation rates and the assumption of the same root-cause for LeTID in areas of different initial τ_{eff} within the Fe+Cu sample.

Considering $N^*(t)$ of the differently contaminated samples, it is possible to fit the degradation data with the same parameters within one sample as described above for the Fe+Cu sample. A comparison of $N^*(t)$ for areas with the same initial τ_{eff} of 50 µs of the differently contaminated samples is shown in Fig. 5. The corresponding fit parameters differ for samples with different impurity species resulting in different defect generation rates. Due to the same initial τ_{eff} in Fig. 5 and the exclusion of a dominating influence of the local defect structure, as discussed above, the calculated differences of the defect generation rates seem to be due to the varying impurities in the investigated materials.

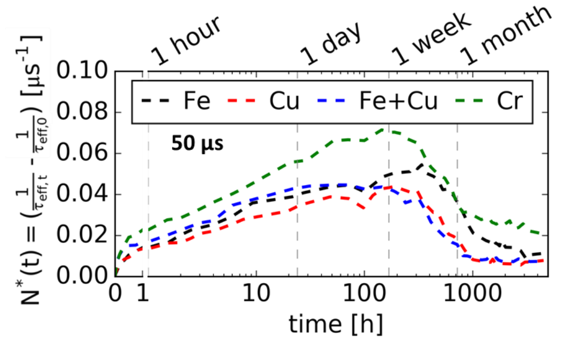

Figure 5: Time-dependent effective defect concentration of the differently contaminated samples with the initial τ_{eff}. of 50 µs.

4 SUMMARY AND DISCUSSION

The influence of different transition metal contaminations on the strength and kinetics of LeTID and regeneration could be shown using data from TR-PLI. Spatially resolved τ_{eff} and harmonic average τ_{eff} have been measured and allow for a separation of degradation and regeneration kinetics in areas of varying material quality. While the lifetime of ungettered samples is so low that LeTID is difficult to observe, P-gettered samples show the known LeTID and regeneration behavior. Areas with the same initial τ_{eff} but different local defect structure show no obvious dependence of LeTID on structural defects.

A comparison of differently contaminated samples shows different LeTID and regeneration kinetics, resulting in different defect generation rates in dependence of the impurity species. The investigated impurities have been excluded as root-cause for LeTID *e.g.* by [12-14], based on their material properties in crystalline Si. It has to be mentioned that material properties like diffusion coefficient are usually

investigated and determined in defect-lean mono-crystalline Si at high temperatures. Therefore, it is reasonable, that those material properties might be different in mc-Si due to its higher (structural) defect density. In defect-rich mc-Si, the diffusion of impurities is influenced by trapping. This might lead to diffusion coefficients varying by several orders of magnitude as it is, *e.g.*, the case for the diffusion of H [14]. Therefore, based on the results discussed above it is still possible that the investigated impurities might be involved in the root-cause of LeTID or at least influence the defect causing LeTID, *e.g.* by trapping H, forming complexes, or changing/influencing recombination activity or charge state.

8 REFERENCES

[1] K. Ramspeck, S. Zimmermann, H. Nagel, A. Metz, Y. Gassenbauer, B. Birkmann, A. Seidl, Proc. 27th EUPVSEC, Frankfurt/Main, Germany, 2012, 861.

[2] F. Fertig, K. Krauss, S. Rein, Physica Status Solidi RRL 9(1) (2014) 41.

[3] F. Kersten, P. Engelhart, H.-C. Ploigt, A. Stekolnikov, T. Lindner, F. Stenzel, M. Bartzsch, A. Szpeth, K. Petter, J. Heitmann, J. Müller, Solar Energy Materials and Solar Cells 142 (2015) 83.

[4] A. Zuschlag, D. Skorka, G. Hahn, Progress in Photovoltaics: Research and Applications 25(7) (2017) 545.

[5] A. Zuschlag, D. Skorka, G. Hahn, Proc. 43rd IEEE PVSC, Portland 2016, 1051.

[6] J. Fritz, A. Zuschlag, D. Skorka, G. Hahn, Energy Procedia 124 (2017) 718.

[7] D. Bredemeier, D. Walter, S. Herlufsen, J. Schmidt, AIP Advances 6 (2016) 035119-1.

[8] A.E. Morishige, M.A. Jensen, D.B. Needleman, K. Nakayashiki, J. Hofstetter, T.-T.A. Li, T. Buonassisi, IEEE Journal of Photovoltaics 6(6) (2016) 1466.

[9] K. Nakayashiki, J. Hofstetter, A. Morishige, T. Li, D. Needleman, M. Jensen, T. Buonassisi, IEEE Journal of Photovoltaics 6(4) (2016) 860.

[10] G. Coletti, P.C.P. Bronsveld, G. Hahn, W. Warta, D. Macdonald, B. Ceccaroli, K. Wambach, N. Le Quang, J.M. Fernandez, Advanced Functional Materials 21 (2011) 879.

[11] S. Riepe, I. Reis, W. Kwapil, M. Falkenberg, J. Schön, H. Behnken, J. Bauer, D. Kreßner-Kiel, W. Seifert, W. Koch, Physica Status Solidi C 8(3) (2011) 733.

[12] D. Kiliani, G. Micard, B. Steuer, B. Raabe, A. Herguth, G. Hahn, Journal of Applied Physics 110 (2011) 054508.

[13] D. Sperber, A. Graf, D. Skorka, A. Herguth, G. Hahn, IEEE Journal of Photovoltaics (2017), accepted, doi: 10.1109/JPHOTOV.2017.2755072.

[14] S. Kleekajai, F. Jiang, M. Stavola, V. Yelundur, K. Nakayashiki, A. Rohatgi, G. Hahn, S. Seren, K. Kalejs, Journal of Applied Physics 100(9) (2006) 093517.